Chemical Transformation Is Not Rate-Limiting in the Reaction Catalyzed by *Escherichia coli* 6-Hydroxymethyl-7,8-dihydropterin Pyrophosphokinase†

Yue Li,‡ Yunchen Gong,‡ Genbin Shi,‡ Jaroslaw Blaszczyk,§ Xinhua Ji,§ and Honggao Yan*,‡

Department of Biochemistry and Molecular Biology, Michigan State University, East Lansing, Michigan 48824, and Macromolecular Crystallography Laboratory, National Cancer Institute, P.O. Box B, Frederick, Maryland 21702

Received April 15, 2002; Revised Manuscript Received May 13, 2002

ABSTRACT: 6-Hydroxymethyl-7,8-dihydropterin pyrophosphokinase (HPPK) catalyzes the transfer of pyrophosphate from ATP to 6-hydroxymethyl-7,8-dihydropterin (HMDP). Because HPPK is essential for microorganisms but is absent from human and animals, the enzyme is an excellent target for developing antimicrobial agent. Thermodynamic analysis shows that Mg^{2+} is important not only for the binding of nucleotides but also for the binding of HMDP. Transient kinetic analysis shows that a step or steps after the chemical transformation are rate-limiting in the reaction catalyzed by HPPK. The pre-steady-state kinetics is composed of a burst phase and a steady-state phase. The rate constant for the burst phase is ∼50 times larger than that for the steady-state phase. The latter is very similar to the k_{cat} value measured by steady-state kinetics. A set of rate constants for the individual steps of the HPPK-catalyzed reaction has been determined by a combination of stopped-flow and quench-flow analyses. These results form a thermodynamic and kinetic framework for dissecting the roles of active site residues in the substrate binding and catalysis by HPPK.

6-Hydroxymethyl-7,8-dihydropterin pyrophosphokinase (HPPK)[1] catalyzes the transfer of pyrophosphate from ATP to 6-hydroxymethyl-7,8-dihydropterin (HMDP, Figure 1), leading to the biosynthesis of folate cofactors (*1*). It belongs to a class of enzymes that catalyze pyrophosphoryl transfer (*2*).

Folate cofactors are essential for life (*3*). Mammals have an active transport system for deriving folates from the diet. In contrast, most microorganisms must synthesize folates de novo because they lack the active transport system. Therefore, the folate biosynthetic pathway is an ideal target for developing antimicrobial agents. Inhibitors of dihydropteroate synthase (DHPS) and dihydrofolate reductase, both of which are enzymes in the folate biosynthetic pathway, are currently used as antibiotics for treating many infectious diseases (*4*). However, the rates of resistance to these antibiotics have increased dramatically during the past 2 decades (*5*). The rapid increase in resistance to these and other antimicrobial agents has caused a worldwide health care crisis (*6*). The crisis is further aggravated by the fact that most of the new antibiotics are chemical modifications of the basic structures of existing antimicrobial agents against old targets and are thus less effective against the widespread antibiotic resistance. New targets for the development of novel antimicrobial agents are thus urgently needed for combating the antibiotic crisis.

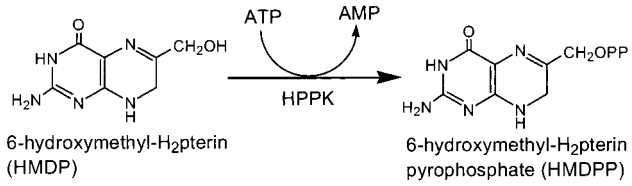

FIGURE 1: Pyrophosphoryl transfer reaction catalyzed by HPPK.

HPPK was first identified in *Escherichia coli* in 1964 (*7*). The gene for *E. coli* HPPK was cloned in 1992 (*8*). The *E. coli* enzyme is highly homologous to HPPKs from many pathogenic microbial organisms. For example, it shares ∼56% identity with *Haemophilus influenzae* HPPK, ∼35% identity with *Staphylococcus aureus* HPPK, and ∼33% identity with *Mycobacterium tuberculosis* HPPK. As a small (158 residues, ∼18 kDa), stable, monomeric protein, *E. coli* HPPK is not only a new target for development of antimicrobial agents but also an excellent model system for studying the catalytic mechanisms of enzymatic pyrophosphoryl transfer.

We are interested in studying the structure−function relationships of HPPK with the aim of elucidating the catalytic mechanisms of the enzyme and providing the critical information for structure-based design of HPPK inhibitors that may become new antimicrobial agents. To these ends, we have recently completed the sequential resonance assignments of HPPK by multidimensional NMR spectroscopy (*9*) and determined its three-dimensional structure by X-ray crystallography (*10*−*12*). Design and synthesis of HPPK inhibitors have also begun (*13*).

† This work was supported in part by NIH Grant GM51901 (H.Y.).

* To whom correspondence should be addressed. Tel: 517-353-8786. Fax: 517-353-9334. E-mail: yanh@msu.edu.

‡ Michigan State University.

§ National Cancer Institute.

[1] Abbreviations: AMPCPP, α,β-methyleneadenosine triphosphate; Ant-ATP, 3′(2′)-*O*-anthraniloyladenosine 5′-triphosphate; DHPS, dihydropteroate synthase; HPPK, 6-hydroxymethyl-7,8-dihydropterin pyrophosphokinase; HMDP, 6-hydroxymethyl-7,8-dihydropterin; HMDPP, 6-hydroxymethyl-7,8-dihydropterin pyrophosphate; pABA, *p*-aminobenzoic acid.

10.1021/bi025968h CCC: $22.00
Published on Web 06/12/2002

Kinetic and mechanistic studies of HPPK lag behind the high-resolution structural work by us (*9*−*12*) and others (*14*, *15*). Recently, Bermingham and co-workers reported transient kinetic analysis of the binding of the substrates to HPPK (*16*), but no transient kinetic analysis of the HPPK-catalyzed reaction has been reported. The rate-determining step in the HPPK-catalyzed reaction is not known. Two Mg^{2+} ions have been identified in the complex of HPPK with AMPCPP (an ATP analogue) and HMDP (*11*), but the roles of Mg^{2+} have not been elucidated. In this paper, we describe the thermodynamic analysis of the binding of HMDP to HPPK and the transient kinetic analysis of the HPPK-catalyzed reaction. The results show that a step or steps after the chemical transformation are rate-limiting in the reaction catalyzed by HPPK and Mg^{2+} is important for the binding of HMDP. The work described in this paper provides a thermodynamic and kinetic framework for dissecting the roles of active site residues in substrate binding and catalysis.

EXPERIMENTAL PROCEDURES

Materials. ATP and AMPCPP were purchased from Sigma. 6-Hydroxymethylpterin (HMP) was synthesized according to the method of Thijssen (*17*) and had the same UV absorption and NMR spectra as that purchased from Sigma. 6-Hydroxymethyl-7,8-dihydropterin (HMDP) was prepared from HMP by reduction with sodium dithionite (*18*) or purchased from Schircks Laboratories. [α-^{32}P]ATP was purchased from NEN. [7-^{14}C]-*p*-Aminobenzoic acid (pABA) was purchased from Moravek. *E. coli* HPPK was purified from the strain BL21(DE3) containing overexpression construct pET17b-HPPK as previously described (*19*). *E. coli* dihydropteroate synthase (DHPS) was purified from the strain BL21(DE3) containing the overexpression construct pET17b-DHPS as previously described (*20*).

Thermodynamic Analysis. Fluorescence measurements of the K_d values for AMPCPP and HMDP were performed on a Spex FluoroMax-2 fluorometer. The titration experiments were performed in a single cuvette so that both protein and ligand concentrations varied with the addition of each aliquot of a stock solution. The independent variable in such an experiment was the volume of the added stock solution. The concentrations of the protein and ligands during the titration could be expressed in terms of the initial concentrations of the titrated solution, the concentration of the stock solution, and the volume of the added stock solution. The AMPCPP titration experiment was carried out as previously described (*19*). Briefly, a solution containing 2 μM HPPK and 2 μM Ant-ATP in 100 mM Tris-HCl and 10 mM $MgCl_2$, pH 8.3, was titrated with AMPCPP at 24 °C. The concentration of the AMPCPP stock solution was 125 μM. The fluorometric data were fitted by a nonlinear least-squares method using the program Origin to eq 1 derived by Wang (*21*).

$$F_{obs} = \epsilon_f A + \frac{(\epsilon_b - \epsilon_f)A\{2\sqrt{(a^2 - 3b)}\cos(\theta/3) - a\}}{3K_A + 2\sqrt{(a^2 - 3b)}\cos(\theta/3) - a} \quad (1)$$

where ϵ_f and ϵ_b are the molar fluorescence intensities for free and bound MgAnt-ATP respectively, A is the concentration of Ant-ATP, and K_A is the dissociation constant for MgAnt-ATP, which was previously determined (*19*). a, b, and θ are defined by the expressions:

$$a = K_A + K_B + A + B - P$$

$$b = K_A(B - P) + K_B(A - P) + K_AK_B$$

$$\theta = \arccos\left(\frac{-2a^3 + 9ab + 27K_AK_B}{2\sqrt{(a^2 - 3b)^3}}\right)$$

where B and P are the concentrations of MgAMPCPP and HPPK, respectively, and K_B is the dissociation constant for MgAMPCPP. The concentrations of A, B, and P vary according to the expressions:

$$A = A_0V_0/(V_0 + \Delta V)$$

$$B = B_0\Delta V/(V_0 + \Delta V)$$

$$P = P_0V_0/(V_0 + \Delta V)$$

where A_0 and P_0 are the initial concentrations of MgAnt-ATP and HPPK, respectively, and B_0 is the concentration of the AMPCPP stock solution.

To determine the K_d value for HMDP, a solution containing 0.11 μM HMDP and 100 μM AMPCPP in 50 mM BICINE, 10 mM $MgCl_2$, and 25 mM DTT, pH 8.3, was titrated with HPPK at 24 °C. The concentration of the HPPK stock solution was 20 μM. The final concentrations of HMDP and HPPK were 0.10 and 1.4 μM, respectively. The fluorescence of HMDP was measured at an emission wavelength of 430 nm with a slit of 10 nm. The excitation wavelength and slit were 330 and 5 nm, respectively. A control titration experiment was performed in the absence of HMDP. The control data set obtained in the absence of HMDP was subtracted from the corresponding data set obtained in the presence of HMDP. The data were then fitted to the equation:

$$F_{obs} = \frac{F_f\Delta V}{V_0 + \Delta V} + \frac{(F_b - F_f)(K_d + E_t + L_t - \sqrt{(K_d + E_t + L_t)^2 - 4E_tL_t})}{2L_t} \quad (2)$$

where F_f and F_b are the fluorescence intensities of free and bound HMDP respectively, F_{obs} is the fluorescence of each titration point, V_0 is the initial volume of the titration, ΔV is the total volume of the added HPPK solution, E_t is the total concentration of HPPK, and L_t is the total concentration of HMDP. E_t and L_t were varied according to the expressions:

$$E_t = E_0\Delta V_0/(V_0 + \Delta V)$$

$$L_t = L_0V_0/(V_0 + \Delta V)$$

where E_0 is the concentration of the HPPK stock solution and L_0 is the initial concentration of HMDP.

Steady-State Kinetics. The HPPK-catalyzed reaction was measured by coupling the reaction to that catalyzed by DHPS. The initial reaction mixtures contained 1.1 nM HPPK, 11 μM DHPS, 20 μM [7-^{14}C]pABA, 10 mM $MgCl_2$, 25 mM DTT, and various amounts of ATP and HMDP in 100 mM

Tris-HCl buffer, pH 8.3. The reaction was initiated by the addition of HPPK at 30 °C and stopped after 10 min of incubation by the addition of an equal volume of 200 mM EDTA and 4 mM unlabeled pABA. The stopped reaction mixture was then incubated for 20 min at 98 °C and separated by ascending chromatography on a sheet of Whatman 3MM paper developed with 0.1 M potassium phosphate, pH 7.0. The radioactivity was quantified by a Molecular Dynamics Storm 820 PhosphorImager. The kinetic parameters were obtained by a nonlinear least-squares fit of the data to the Michaelis−Menten equation using the program Origin from Microcal.

Stopped-Flow Analysis. Stopped-flow experiments were performed in an Applied Photophysics SX.18MV-R stopped-flow spectrofluorometer. To measure the binding of MgATP, a solution containing HPPK was mixed rapidly with a solution containing ATP and $MgCl_2$ at 26 °C. Fluorescence traces were obtained with an excitation wavelength of 295 nm and a filter with a cutoff of 320 nm for emission. HPPK and $MgCl_2$ were fixed at 2 μM and 10 mM, respectively. ATP was varied from 2.5 to 20 μM. To measure the binding of HMDP, a solution containing HPPK, AMPCPP, and $MgCl_2$ was mixed rapidly with a solution containing HMDP at 26 °C. The fluorescence traces were obtained with an excitation wavelength of 330 nm and a filter with a cutoff of 395 nm for emission. HPPK, AMPCPP, and $MgCl_2$ were fixed at 0.2 μM, 25 μM, and 10 mM, respectively. HMDP was varied from 0.125 to 1 μM. All concentrations refer to the concentrations right after the rapid mixing. The rate constants were evaluated by numerical analysis of the stopped-flow data using the program DYNAFIT (*22*). The initial values for the iterative numerical analysis were obtained by a nonlinear least-squares fit of the stopped-flow data to an exponential equation using the program Origin.

Quench-Flow Analysis. All quench-flow experiments were carried out with a KinTek RQF-3 rapid quench-flow instrument. All reaction components were dissolved in 100 mM Tris-HCl buffer, pH 8.3. A trace amount of [α-^{32}P]ATP was used to follow the reactions. The reactions were initiated with Mg^{2+} at 30 °C and quenched with 500 mM EDTA. The substrates and products were separated by thin-layer chromatography on a plastic sheet coated with PEI−cellulose developed with 0.25 M NaH_2PO_4. The radioactivity was quantified by a Molecular Dynamics Storm 820 Phosphor-Imager as in the steady-state kinetic experiments. In pre-steady-state experiments, the reaction mixture contained 10 μM HPPK, 100 μM ATP, 55−275 μM HMDP, 25 mM DTT, 0.5 mM EDTA, and 10 mM $MgCl_2$ in 100 mM Tris-HCl buffer, pH 8.3. In single-turnover experiments, the reaction mixture contained 20 μM HPPK, 100 μM ATP, 2.2 μM HMDP, 25 mM DTT, 0.5 mM EDTA, and 10 mM $MgCl_2$ in 100 mM Tris-HCl buffer, pH 8.3. The pre-steady-state and single-turnover data were first analyzed by a nonlinear least-squares fit of the data to eqs 3 and 4, respectively. The amplitudes and rate constants were then used to set the initial values for fitting the data to the complete mechanism by numerical analysis using the program DYNAFIT (*22*).

$$[\text{AMP}]/[\text{HPPK}] = A(1 - e^{\lambda_1}) + k_{\text{cat}}t \quad (3)$$

$$[\text{AMP}] = B(1 - e^{\lambda_1}) \quad (4)$$

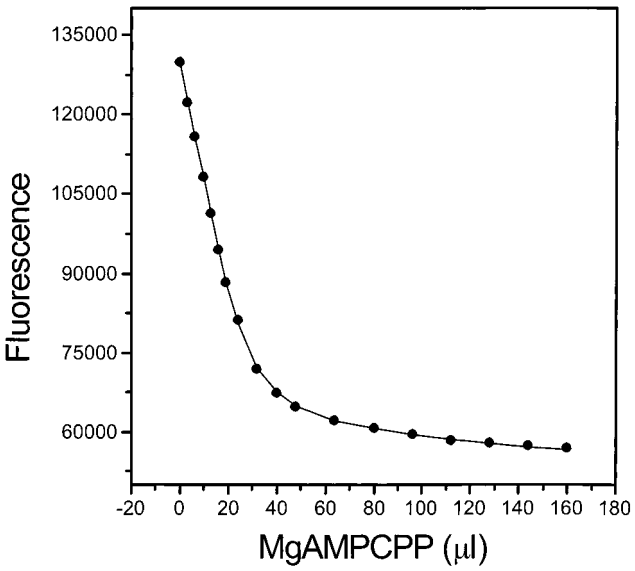

FIGURE 2: Competitive binding of AMPCPP to HPPK measured by fluorometry. The final concentrations of AntATP, AMPCPP, and HPPK were 1.9, 9.3, and 1.9 μM, respectively. The solid line was obtained by a nonlinear least-squares fit to eq 1 as described under Experimental Procedures.

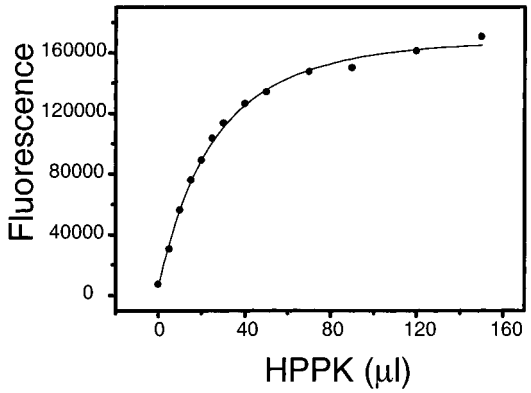

FIGURE 3: Binding of HMDP to HPPK measured by fluorometry. The final concentrations of HMDP and HPPK were 0.10 and 1.4 μM, respectively. The solid line was obtained by a nonlinear least-squares fit to eq 2 as described under Experimental Procedures.

RESULTS

Thermodynamic Analysis. Recently, we reported the thermodynamic analysis of the nucleotide-binding properties of HPPK (*19*). In this study, we performed the thermodynamic analysis of the pterin-binding properties of HPPK. The binding studies were performed in the presence of a nucleotide triphosphate (ATP or its analogue AMPCPP), because we found that pterin compounds had much higher affinity for an HPPK−nucleotide complex than for the free HPPK, in agreement with the recent report by Bermingham and co-workers (*16*). First, we determined the K_d value of AMPCPP using a competitive binding assay previously developed in our laboratory (*19*) (Figure 2). It was 0.077 ± 0.006 μM (an average of five measurements) in the presence of 10 mM $MgCl_2$, corresponding to a Gibbs free energy change of 9.7 kcal/mol. Then we determined the affinity of HMDP for HPPK in the presence of 100 μM AMPCPP and 10 mM $MgCl_2$ (Figure 3). Under such conditions, >99.9% of HPPK was in complex with MgAMPCPP. Thus, only the formation of the ternary complex HPPK·Mg_2AMPCPP·

Table 1: Binding Properties of HPPK

	K_d (μM)	ΔG (kcal/mol)
MgAMPCPP	0.077 ± 0.006	−9.7
MgATP[a]	2.6 ± 0.06	−7.6
ATP[a]	38 ± 2.7	−6.0
AMP[a]	140 ± 11	−5.3
HMDP[b]	0.17 ± 0.01	−9.2
HMDP[c]	110 ± 17	−5.4
HMDP[d]	89 ± 14	−5.5

[a] From Shi et al. (*19*). [b] Measured in the presence of 100 μM AMPCPP and 10 mM $MgCl_2$. [c] Measured in the presence of 1 mM AMPCPP and 0.5 mM EDTA. [d] Measured in the presence of 1 mM ATP and 0.5 mM EDTA.

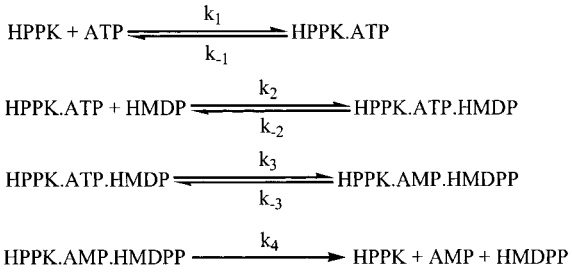

FIGURE 4: Kinetic mechanism of HPPK. Mg^{2+} is required for the reaction, but for simplicity, Mg^{2+} is not shown in the scheme.

HMDP needed to be considered for the nonlinear least-squares analysis of the titration data. The K_d value for HMDP was obtained by a nonlinear fit of the titration data to eq 2 derived from a one-to-one binding model. It was 0.17 ± 0.01 μM (an average of five measurements), corresponding to a Gibbs free energy change of 9.2 kcal/mol. The K_d value for the binary complex is in the millimolar range (*10*). In the absence of Mg^{2+}, the K_d value for HMDP was 110 ± 17 μM, ~650 times that in the presence of Mg^{2+}. In the presence of ATP (without Mg^{2+}), the K_d value for HMDP was 89 ± 14 μM, very similar to that in the presence of AMPCPP. The values of the various dissociation constants are summarized in Table 1. The K_d value for MgAMPCPP measured by us is lower than that (0.45 μM) reported by Bermingham and co-workers (*16*), but the K_d value for HMDP measured by us is higher than that (0.036 μM) reported by Bermingham and co-workers (*16*). The differences are probably due to different experiment conditions. For example, the Mg^{2+} concentration was 10 mM in our experiments but was 2.5 mM in the experiments reported by Bermingham and co-workers (*16*). We chose the higher Mg^{2+} concentration for our experiments because the maximum rate was achieved with ~5 mM Mg^{2+} and higher concentrations of Mg^{2+} did not show inhibitory effects (*23*).

Kinetic Analysis. The kinetics of the HPPK-catalyzed reaction follows apparently an ordered mechanism as depicted in Figure 4 (*16*). Bermingham and co-workers have shown by stopped-flow fluorometric analysis that the fluorescence change of HMDP follows the slow binding of AMPCPP if HMDP, HPPK, AMPCPP, and Mg^{2+} are mixed at the same time, but the fluorescence change follows a fast course if HPPK, AMPCPP, and Mg^{2+} are mixed first (*16*). The interpretation was that HMDP binds only to the binary complex of HPPK and MgAMPCPP, and the binding of MgAMPCPP to HPPK is slow and is followed by the rapid addition of HMDP to the binary complex. The rate constants for the binding of the two substrates, ATP and HMDP,

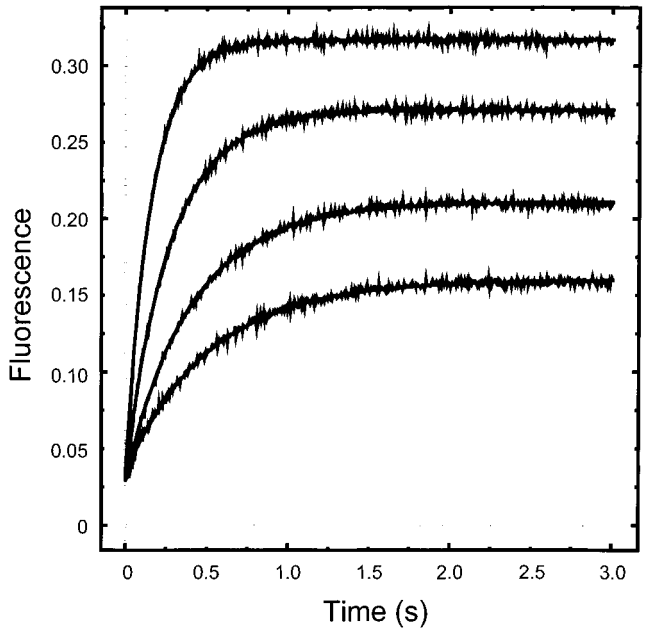

FIGURE 5: Transient kinetic analysis of binding of ATP. The concentrations of HPPK and $MgCl_2$ were fixed at 2 μM and 10 mM, respectively. The concentrations of ATP were 2.5, 5, 10, and 20 μM for the traces from bottom to top, respectively. All concentrations refer to the concentrations right after the rapid mixing. The solid lines were obtained by global fitting using the program DYNAFIT (*22*).

however, have not been measured. To determine the rate constants of individual steps in the reaction, a combination of stopped-flow and quench-flow analyses was performed. The binding of MgATP was monitored by the tryptophan fluorescence of HPPK. Although the fluorescence change was relatively small, it was significant and sufficient for the kinetic analysis (Figure 5). Global fitting using the program DYNAFIT gave the association rate constant (k_1) of 0.27 ± 0.001 μM^{-1} s^{-1} and the dissociation rate constant of 0.95 ± 0.001 (k_{-1}) s^{-1}, similar to those for MgMANT-ATP (a fluorescent analogue of MgATP) measured by Bermingham and co-workers (*16*). The K_d for MgATP calculated from the kinetic constants was 3.5 μM, comparable to that (2.6 μM, Table 1) determined previously by equilibrium measurement (*19*). The binding of HMDP to HPPK was measured again in the presence of AMPCPP and Mg^{2+}. HPPK was mixed with AMPCPP and Mg^{2+} first and incubated in one syringe before being mixed with the HMDP solution in the other syringe. The concentration of AMPCPP was sufficient to saturate HPPK. The complex of HPPK with AMPCPP and Mg^{2+} was formed first so that what we measured was the rapid binding of HMDP, not the slow binding of AMPCPP. The transient kinetic traces are shown in Figure 6. The association and dissociation rate constants obtained by global fitting were 11 ± 0.03 μM^{-1} s^{-1} and 2.0 ± 0.004 s^{-1}, respectively. The association rate constant for HMDP was ~40 times that for the binding of MgATP, consistent with the rapid binding of HMDP observed by Bermingham and co-workers (*16*). The K_d for HMDP calculated from the rate constants was 0.18 μM, in close agreement with that measured by the equilibrium measurement described earlier.

While the stopped-flow analysis was convenient for measuring the kinetics of the binding of the substrates to HPPK, the quench-flow analysis was more accurate for

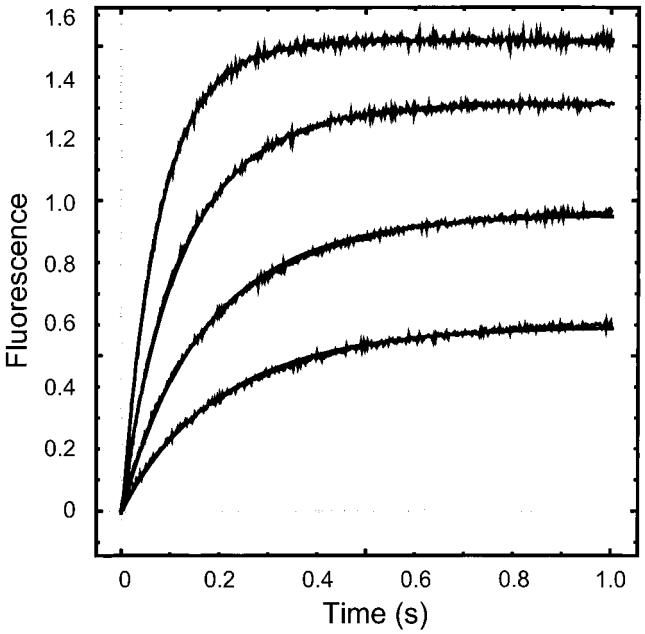

FIGURE 6: Transient kinetic analysis of binding of HMDP. The concentrations of HPPK, AMPCPP, and $MgCl_2$ were fixed at 0.2 μM, 25 μM, and 10 mM, respectively. The concentrations of HMDP were 0.125, 0.25, 0.5, and 1 μM for the traces from bottom to top, respectively. The solid lines were obtained by global fitting using the program DYNAFIT (*22*).

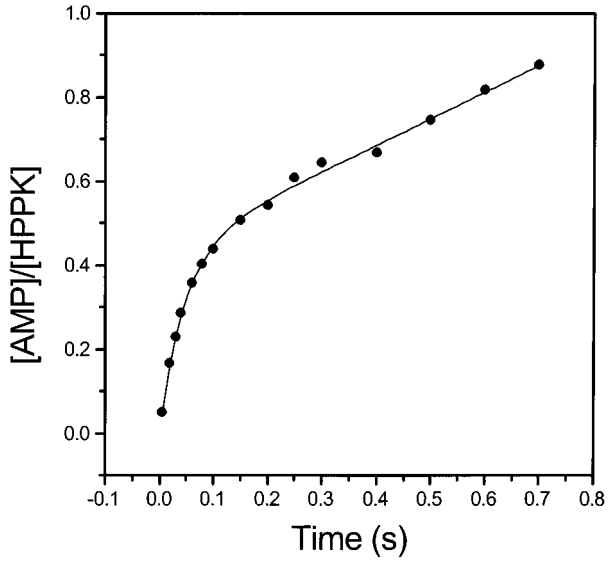

FIGURE 7: Burst kinetics of the HPPK-catalyzed reaction. The reaction mixture contained 10 μM HPPK, 100 μM ATP, 55 μM HMDP, 25 mM DTT, 0.5 mM EDTA, and 10 mM $MgCl_2$. The solid lines were obtained by a nonlinear least-squares fit to eq 3 as described under Experimental Procedures.

measuring the kinetics of the chemical step. To measure the rate constants for the HPPK-catalyzed reaction, a series of quench-flow experiments were carried out. Global analysis was then used to get the best estimation of the rate constants by fitting all of the data to the complete kinetic mechanism using one set of rate constants. Our analysis began with pre-steady-state experiments with both substrates in large excess with respect to the enzyme. The reaction was initiated by mixing with Mg^{2+}. The result of a representative pre-steady-state kinetic experiment is shown in Figure 7. In the experiment, HPPK was saturated with both substrates. The reaction rate was not limited by the steps toward the formation of the substrate ternary complex as increasing the concentration of either substrate or Mg^{2+} did not increase the reaction rate (data not shown). The pre-steady-state kinetics could be described by Scheme 1 and eq 3.

Scheme 1

$$\text{HPPK}\cdot\text{ATP}\cdot\text{HMDP} \underset{k_{-3}}{\overset{k_3}{\rightleftharpoons}} \text{HPPK}\cdot\text{AMP}\cdot\text{HMDPP} \xrightarrow{k_4} \text{HPPK} + \text{ATP} + \text{HMDPP}$$

As shown in Figure 7, the reaction consisted of two phases, a burst phase and a steady-state phase. The burst phase was characterized by two constants, the amplitude A and the rate constant λ. The steady-state phase was characterized by the rate constant k_{cat}. The three constants were related to the rate constants in Scheme 1 according to the equations (*24*):

$$A = \frac{k_3(k_3 + k_{-3})}{(k_3 + k_{-3} + k_4)^2} \quad (5)$$

$$\lambda = k_3 + k_{-3} + k_4 \quad (6)$$

$$k_{cat} = \frac{k_3 k_4}{k_3 + k_{-3} + k_4} \quad (7)$$

The amplitude and rate constants for the two phases of the reaction were evaluated by a nonlinear least-squares fit to eq 3. The rate constants in Scheme 1 were then estimated according to eqs 5−7 and used to set the initial values for the numerical analysis using the program DYNAFIT (*22*) to obtain more precise values for the individual rate constants. The average values of nine measurements were 16 ± 1, 20 ± 1, and 1.8 ± 0.1 s^{-1} for k_3, k_{-3}, and k_4 respectively. The k_{cat} value calculated according to eq 7 was 0.76 s^{-1}, in close agreement with that (0.71 ± 0.06 s^{-1}) measured by the steady-state kinetic experiments. The rate constant for the burst phase ($k_3 + k_{-3} + k_4$) is ~50 times larger than that for the steady-state phase (k_{cat}).

The rate constants for the burst phase of the reaction were further evaluated by single-turnover experiments (Figure 8). In the single-turnover experiments, HPPK (20 μM) was saturated with MgATP (100 μM) but was in excess with respect to HMDP (2.2 μM). The reaction was characterized by a single exponential term with a rate constant of 35 ± 4 s^{-1} and an amplitude of 0.94 ± 0.06 μM (an average of nine experiments). The rate constant for the single-turnover experiment was very close to the sum of the forward and reverse rate constants for the burst phase of the reaction in the pre-steady-state experiments, indicating that the reaction rapidly reached a quasi-equilibrium between an enzyme−substrate complex and an enzyme−product complex. The rate constants (k_2 and k_{-2}) for the binding of HMDP to the binary complex of HPPK and MgATP were evaluated by quench-flow experiments varying HMDP (2−9 μM while HPPK and MgATP were fixed at 2 and 40 μM, respectively). The values for k_2 and k_{-2} obtained by global analysis of the data (not shown) were 17 ± 0.7 μM s^{-1} and 3.1 ± 0.1 s^{-1}, respectively, similar to the corresponding rate constants for the binding of HMDP to the binary complex of HPPK and MgAMPCPP. The K_d calculated from the rate constants was the same as that calculated from the rate constants for the

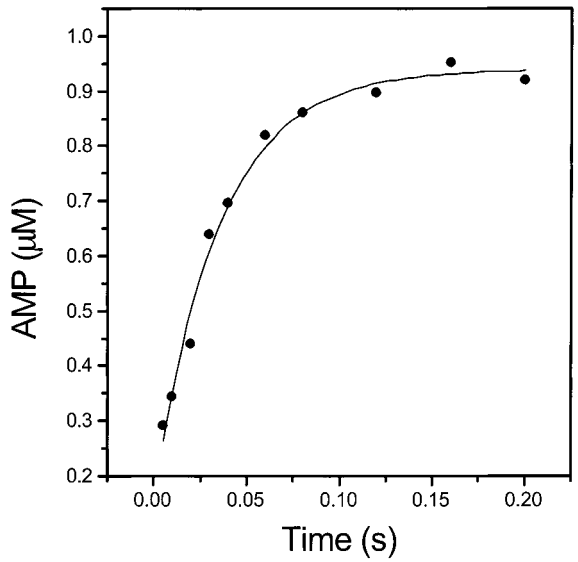

FIGURE 8: HPPK single-turnover kinetics. The reaction mixture contained 20 μM HPPK, 100 μM ATP, 2.2 μM HMDP, 25 mM DTT, 0.5 mM EDTA, and 10 mM $MgCl_2$ in 100 mM Tris-HCl buffer, pH 8.3. The solid lines were obtained by a nonlinear least-squares fit to eq 4 as described under Experimental Procedures.

Table 2: Kinetic Constants of the Reaction Catalyzed by HPPK[a]

k_1	0.27 ± 0.001 μM s^{-1}	k_{-1}	0.95 ± 0.001 s^{-1}
k_2	17 ± 0.7 μM s^{-1}	k_{-2}	3.1 ± 0.1 s^{-1}
k_3	16 ± 1 s^{-1}	k_{-3}	20 ± 1 s^{-1}
k_4	1.8 ± 0.1 s^{-1}	k_{cat}	0.71 ± 0.06 s^{-1}

[a] The rate constants for individual steps are defined in Figure 4. The values for k_1 and k_{-1} were obtained by stopped-flow analysis and were fixed during the global fitting of the pre-steady-state quench-flow data. The rate constants k_2, k_{-2}, k_3, k_{-3}, and k_4 were determined by quench-flow analysis. k_{cat} was measured by steady-state kinetic experiments. Because only high concentrations of substrates were used in the steady-state kinetic experiments due to experimental constraints, the K_m values were not accurate and therefore are not listed in this table.

binding of HMDP to the binary complex of HPPK and MgAMPCPP. The values for all of the rate constants defined by Figure 4 are summarized in Table 2.

DISCUSSION

Chemistry Is Not Rate-Limiting in the Reaction Catalyzed by E. coli HPPK. Bermingham and co-workers have reported transient kinetic analysis of the binding of the substrates to HPPK, but the rate constants for the binding of the substrates have not been determined (*16*). No transient kinetic analysis of the chemical reaction has been reported. In this study, we have determined for the first time a set of rate constants for the HPPK-catalyzed reaction.

Unlike the phosphoryl transfer reactions catalyzed by kinases, which take place at the Pγ atom of ATP, the pyrophosphoryl transfer reaction catalyzed by HPPK takes place at Pβ of ATP. Nucleophilic substitutions at Pβ are thought to be intrinsically more difficult than at Pα and Pγ because of the greater electron density at Pβ. Thus the enzymes that catalyze pyrophosphoryl transfer have low k_{cat} values (*25*). Indeed, the k_{cat} of *E. coli* HPPK is only 0.71 s^{-1}. However, the transient kinetic experiments reported here clearly indicate that a step or steps after the chemical transformation are rate-limiting in the reaction catalyzed by HPPK. The pre-steady-state kinetics is composed of two phases, a burst phase and a steady-state phase. The burst phase is due to the rapid formation of the product complex. Either the forward or the reverse rate constant for the chemical step (k_3 or k_{-3}) is >20 times the rate constant for the steady-state phase (k_{cat}). The chemical step of the HPPK-catalyzed reaction is relatively fast. Thus, the small k_{cat} of HPPK is not due to the chemical step but rather due to a slow step or steps after the pyrophosphoryl transfer.

What is the rate-limiting step? It could be due to slow release of the products. If that is the case, the release of the product HMDPP is most likely the rate-limiting step. With a K_d of 0.18 μM (calculated from k_2 and k_{-2}), the substrate HMDP has a high affinity for the binary complex of HPPK and MgATP. The pyrophosphorylated product HMDPP might have an even higher affinity for HPPK and, consequently, is slow to leave the product complex. On the other hand, the other product AMP has a low affinity for HPPK with a K_d of 140 μM (*19*). Assuming the association rate constant for AMP is on the order of 1 μM s^{-1}, the dissociation rate constant for AMP is then on the order of 100 s^{-1}. Thus the release of AMP is probably not a rate-limiting step.

The small k_{cat} could also be due to a slow conformational change step after the chemical transformation. The idea is consistent with the observations made from a comparison of the crystal structures of the unligated HPPK (*10*) and its complex with HMDP, AMPCPP, and two Mg^{2+} ions (*11*). As revealed by the crystal structures, the formation of the ternary complex involves coupled movements of three catalytic loops (*11*). The active center of HPPK is sealed upon the formation of the ternary complex HPPK·Mg_2AMPCPP·HMDP. The bound HMDP is completely buried in the active center. Thus, the release of the products must involve the opening of the active center. The opening of the active center could be rate-limiting if it is slow relative to the chemical step. The two possibilities are not mutually exclusive. Indeed, a slow conformational change may cause the slow release of the products.

Mg^{2+} Plays an Important Role throughout the Catalytic Cycle. Richey and Brown showed that Mg^{2+} is required for the HPPK-catalyzed reaction (*23*). Two Mg^{2+} ions have been found in the crystal structures of the ternary complexes of HPPK, one coordinated with the α- and β-phosphate and the other with β- and γ-phosphate (*11*). Each Mg^{2+} is also coordinated with the carboxyl groups of Asp95 and Asp97. One of the two Mg^{2+} ions is also coordinated with the hydroxyl oxygen of HMDP.

Previously, we showed that Mg^{2+} is important for the binding of ATP. The ratio of the K_d's of ATP in the absence and the presence of 10 mM $MgCl_2$ is ~15 (*19*). Mg^{2+} is involved in the movement of catalytically important loop 3 upon the binding of ATP (*12*). The present study showed that Mg^{2+} is even more important for the binding of HMDP. The ratio of the K_d's of HMDP measured in the presence of AMPCPP but without $MgCl_2$ to that measured in the presence of both AMPCPP and $MgCl_2$ is ~650. The dissociation constant of HMDP in the presence of both ATP and $MgCl_2$ cannot be measured by equilibrium methods because of the unavoidable chemical reaction, but it can be calculated from the association and dissociation rate constants (k_2 and k_{-2}, respectively) measured by the transient kinetic experiments. The ratio of the dissociation constant of HMDP measured

in the presence of ATP but without $MgCl_2$ to that calculated from k_2 and k_{-2} for the binding of HMDP to HPPK in the presence of both ATP and $MgCl_2$ is ~500, suggesting a critical role of Mg^{2+} in the binding of HMDP. The bound HMDP in HPPK is sandwiched between the aromatic rings of Tyr53 and Phe123 and is held with as many as six hydrogen bonds and the coordination with one of the two bound Mg^{2+} ions (*10*). Although the HMDP-binding pocket in the free enzyme is not blocked, all of the groups that form hydrogen bonds with HMDP are not in the positions to form hydrogen bonds with HMDP. Thus Mg^{2+} may play an important role in the binding of HMDP through direct coordination with HMDP and/or an induced fit mechanism that brings the side chains of the active site residues for hydrogen bonding with HMDP.

ACKNOWLEDGMENT

We thank Ms. Yan Wu for expert technical assistance, Mr. Richard Fielding for assistance in acquiring the stopped-flow data, and Dr. Zachary Burton for critical reading of the manuscript.

REFERENCES

1. Shiota, T. (1984) in *Chemistry and Biochemistry of Folates* (Blakley, R. T., and Benkovic, S. J., Eds.) pp 121−134, John Wiley & Sons, New York.
2. Switzer, R. L. (1974) in *The Enzymes* (Boyer, P., Ed.) pp 607−629, Academic Press, New York.
3. Blakley, R. L., and Benkovic, S. J. (1984) *Folates and Pterins*, John Wiley & Sons, New York.
4. O'Grady, F., Lambert, H. P., Finch, R. G., and Greenwood, D. (1997) *Antibiotic and Chemotherapy: Anti-Infective Agents and Their Use in Therapy*, 7th ed., Churchill Livingstone, New York.
5. Huovinen, P. (1997) *Clin. Infect. Dis. 24*, S63−S66.
6. Murray, B. E. (1997) *Adv. Intern. Med. 42*, 339−367.
7. Weisman, R. A., and Brown, G. M. (1964) *J. Biol. Chem. 239*, 326−331.
8. Talarico, T. L., Ray, P. H., Dev, I. K., Merrill, B. M., and Dallas, W. S. (1992) *J. Bacteriol. 174*, 5971−5977.
9. Shi, G., Gao, J., and Yan, H. (1999) *J. Biomol. NMR 14*, 189−190.
10. Xiao, B., Shi, G., Chen, X., Yan, H., and Ji, X. (1999) *Structure 7*, 489−496.
11. Blaszczyk, J., Shi, G., Yan, H., and Ji, X. (2000) *Structure 8*, 1049−1058.
12. Xiao, B., Shi, G., Gao, J., Blaszczyk, J., Liu, Q., Ji, X., and Yan, H. (2001) *J. Biol. Chem. 276*, 40274−40281.
13. Shi, G., Blaszczyk, J., Ji, X., and Yan, H. (2001) *J. Med. Chem. 44*, 1364−1371.
14. Hennig, M., Dale, G. E., D'Arcy, A., Danel, F., Fischer, S., Gray, C. P., Jolidon, S., Müller, F., Page, M. G. P., Pattison, P., and Oefner, C. (1999) *J. Mol. Biol. 287*, 211−219.
15. Stammers, D. K., Achari, A., Somers, D. O., Bryant, P. K., Rosemond, J., Scott, D. L., and Champness, J. N. (1999) *FEBS Lett. 456*, 49−53.
16. Bermingham, A., Bottomley, J. R., Primrose, W. U., and Derrick, J. P. (2000) *J. Biol. Chem. 275*, 17962−17967.
17. Thijjssen, H. H. W. (1973) *Anal. Biochem. 54*, 609−611.
18. Scrimgeour, K. G. (1980) *Methods Enzymol. 66*, 517−523.
19. Shi, G., Gong, Y., Savchenko, A., Zeikus, J. G., Xiao, B., Ji, X., and Yan, H. (2000) *Biochim. Biophys. Acta 1478*, 289−299.
20. Dallas, W. S., Crowen, J. E., Ray, P. H., Cox, M. J., and Dev, I. K. (1992) *J. Bacteriol. 174*, 5961−5970.
21. Wang, Z.-X. (1995) *FEBS Lett. 360*, 111−114.
22. Kuzmic, P. (1996) *Anal. Biochem. 237*, 260−273.
23. Richey, D. P., and Brown, G. M. (1969) *J. Biol. Chem. 244*, 1582−1592.
24. Johnson, K. A. (1992) in *The Enzymes* (Sigman, D. S., Ed.) pp 1−61, Academic Press, San Diego.
25. Mildvan, A. S., Weber, D. J., and Abeygunawrdana, C. (1999) *Adv. Enzymol. Relat. Areas Mol. Biol. 73*, 183−207.

BI025968H